ARTICLE TYPE www.rsc.org/xxxxxx | XXXXXXXX

Quantised Charging of Monolayer-Protected Nanoparticles

Timo Laaksonen,[a] Virginia Ruiz,[b] Peter Liljeroth[c] and Bernadette M. Quinn[d*]

Received (in XXX, XXX) 1st January 2007, Accepted 1st January 2007
First published on the web 1st January 2007
DOI: 10.1039/b000000x

Metal nanoparticles coated with an organic monolayer, so-called monolayer protected clusters (MPCs), can show quantised charging at room temperature due to their sub-aF capacitance arising from the core size and the nature of the protecting monolayer. In this tutorial review, we treat the factors affecting the energetics of MPC charging. In the first section, the underlying physics of quantised charging is outlined and we give an overview of the various methods that can be used to measure single electron transfer to nanoparticles. In the subsequent sections, we discuss how electrochemical measurements can be used to give information on the quantised charging of freely diffusing and films of immobilised MPCs. The predictions of models used to determine MPC capacitance are compared with experimental data from the literature.

Introduction

During the past decade, the synthesis and properties of metallic and semiconductor nanocrystals have been the focus of both academic and technological interest. These novel materials lie between the molecular and solid-state regimes and have exciting properties controlled by the size and shape of the nanocrystals. The most common example of these size-dependent properties is the quantum confinement effect in semiconductor nanocrystals (quantum dots, QD). As illustrated in Figure 1a, when the size of the crystal is reduced to nanometre dimensions, the energy bands of the bulk semiconductor split to discrete levels, the conduction (electron) and valence (hole) levels.[1] Eventually, the situation of an isolated atom is recovered, where the highest occupied molecular orbital (HOMO) is filled with two electrons. Semiconductor QDs are an experimental realisation of the text-book "particle in a box" problem in quantum mechanics; added electrons occupy orbitals with atom-like symmetries. The wave function of the first added electron has no nodal plane (S symmetry). This level can accommodate a second electron, with opposite spin. A third electron will occupy the next higher energy level, which has one nodal plane and P-type symmetry. Such few-electron configurations confined in semiconductor nanocrystals are known as artificial atoms.[2]

The synthesis methods available to obtain monodisperse QDs of controlled size and shape are very advanced and this has accelerated fundamental understanding of their size dependent properties.[3] The lack of comparable synthesis routes to generate isolable metal nanoparticles was a major obstacle to studying their properties. Although surfactant stabilized metal colloids have been used since medieval times to stain glass, their electronic properties had not been studied in detail due to the difficulty in isolating the particles from the excess surfactant. In elegant early experiments, Henglein and co-workers demonstrated that metal colloids can act as electron donors or acceptors in pulse radiolysis experiments.[4] However, the generated charged nanoparticles were not sufficiently stable for in depth characterisation. The breakthrough was the seminal contribution from Brust,

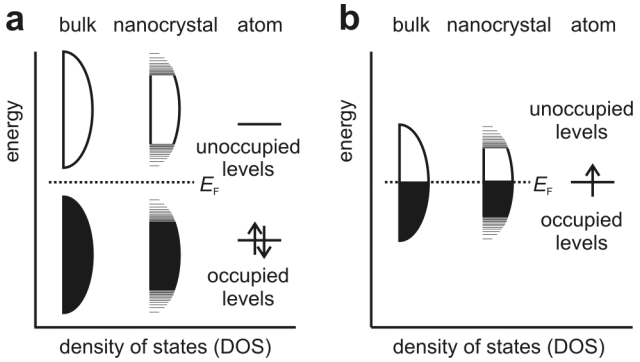

Fig. 1 Evolution of the density of states going from bulk (left) to nanocrystal (middle) to an isolated atom (right) for (a) semiconducting and (b) metallic materials. Adapted from Ref. 1.

Schiffrin and co-workers who reported a simple two-phase synthesis of alkanethiol protected gold nanoparticles.[5] The synthesis differed from other preparation methods in that the generated particles could be purified and were stable both in solution and dry form indefinitely. A monolayer of alkanethiols protects the metal core from agglomerating in solution allowing the particles to be treated as regular chemical reagents. Nanoparticles of this type are termed monolayer-protected clusters (MPCs) in the literature.[6]

The simple synthesis method and the stability of the resulting particles lead to the development of a new field of research.[6, 7] As the particles could be size-selected, their electronic and optical properties could be unambiguously studied as a function of the core size. Unlike semiconductors, the highest occupied band in bulk metal is half-filled, thus electrons can be excited thermally or by an electric field giving rise to metallic properties of the crystal. The Fermi level is in the middle of the band, where the density of state (DOS) is highest. Thus, to observe discrete energy levels, the crystal size must be made correspondingly smaller. This is illustrated schematically in Figure 1b where it can be seen how the DOS evolves going from a bulk metal to an isolated atom. To get an idea of the difference between semiconducting and metallic nanocrystals, we note that in

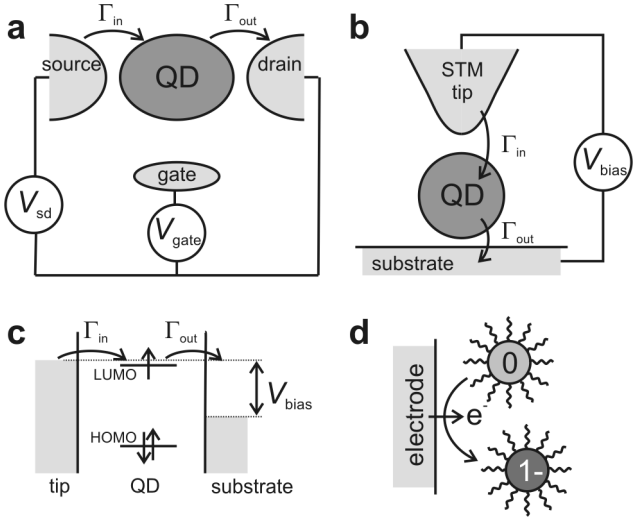

Fig. 2 Schematics of different experimental setups used to measure energy levels and charging energies of nanocrystals. (a) Schematic of a three-terminal (source-drain-gate) device where the energy levels are probed by measuring the current between the source and drain electrodes at small bias as a function of the voltage at the gate electrode, which is capacitively coupled to the system under investigation (no current) and can be used to change the electrochemical potential of the QD. Γ_{in} and Γ_{out} denote the tunnelling rates in and out of the QD. (b) Schematic of tunnelling spectroscopy of a QD using an STM: the STM tip is fixed above the QD of interest and the current is measured as a function of the bias voltage between the tip and the substrate. (c) Energy level diagram of the STM set-up which shows how electron transport is possible when the tip Fermi level aligns with an energy level of the QD. (d) Schematic of the electrochemical measurement of electron addition to MPCs. The electrode potential is controlled with respect to the reference electrode and this drives electron transfer from the electrode to the MPCs that are dispersed in an electrolyte solution.

PbSe, discrete energy levels can be observed in nanocrystals with a diameter of over 10 nm whereas with gold, nanocrystals with a radius of 1.5 nm still have essentially continuous DOS around the Fermi level. Finally, in contrast to semiconductor QDs where the first added electron to the conduction levels is an experimental realization of the particle in a box problem, metallic nanoclusters correspond to the N particles in a box problem, where N is the number of atoms in the cluster (for 1 conduction electron per atom).

Although quantum confinement effects are only seen for sub-nanometre metal cores, larger cores can show discrete charging simply as a consequence of the nm core size and nature of the protecting monolayer.[8] This quantised charging can be observed at room temperature and has been the focus of intense interest.[7] In this review, we explain why this quantised charging is observed for MPCs and how electrochemical experiments can be used to give analogous information to traditional electron transport experiments. We will discuss the factors influencing the energetics of the single electron charging and how they can be rationalised with a physical model of the MPC. We look at both freely diffusing MPCs and those immobilised on an electrode surface. It will be shown that in both instances, the MPCs behave as redox mediators in classical electrochemical measurements.

Probing energy levels in nanocrystals

When we consider the energetics of electron addition to small crystals, the response is determined by three different energy scales.[2, 9] The effect of quantum confinement is manifest in the spacing of the electronic levels ΔE. Furthermore, in small crystals, Coulomb repulsion between added electrons results in a considerable energy cost E_c. The third relevant energy scale is the thermal energy kT. By comparing these energies, we can classify the behaviour of small crystals. If ΔE and E_c are both smaller than kT, the behaviour is the same as in the bulk. In metal nanocrystals, it is common to have E_c that is considerably larger than either ΔE or kT: then the response is determined by Coulomb blockade as explained in the following section. In semiconductor nanocrystals and very small metal clusters, both ΔE and E_c are larger than kT and will affect the observed response of the system.

Energy levels and the charging energies of single nanocrystals can be probed electrically either in a three-terminal (source, drain, gate) device configuration (Figure 2a) fabricated using lithographic techniques or in a two-terminal setup using the tip of a scanning tunnelling microscope (STM) as one of the electrodes (Figure 2b).[10-13] In both cases, the system can be considered as a double-barrier tunnelling junction, where the resistance of the barriers is much higher than the quantum of resistance $h/2e^2$, i.e. the nanocrystal is weakly electronically coupled to the leads (electrodes). In this case, the physics of the electron transport is described by the so-called orthodox theory of single-electron tunneling.[9] The high resistance of the barriers is crucial as it ensures that nanocrystal has a well-defined number of added electrons, i.e. there is no quantum uncertainty in the electron occupation.

In the three-terminal devices, the gate electrode sets the electrochemical potential of the electrons in the nanocrystal and hence, the number of added electrons.[2, 10] The tunnelling rates, Γ, between the dot and the electrodes are usually similar (symmetric junction) and bias voltage (potential difference between the source and the drain) is kept small. Electron transport between the source and the drain is possible when there is an energy level in the nanocrystal between the Fermi levels of the source and the drain.

In the STM configuration, the tunnelling rate between the particle and the substrate (Γ_{out}) is fixed by the geometry of that junction while the tunnelling rate between the tip and the dot (Γ_{in}) can be modified by moving the tip closer or farther from the nanocrystal. Normally, the junction is asymmetric ($\Gamma_{in} \neq \Gamma_{out}$) and this has a profound effect on the transport through the system. In the limiting case of $\Gamma_{in} << \Gamma_{out}$ (this is called shell-tunnelling), the electrons tunnel through the nanocrystal one-by-one and electron-electron interactions are absent.[13, 14] In this case, the average number of added electrons in the nanocrystal is zero. In the other limiting case called shell-filling, $\Gamma_{in} >> \Gamma_{out}$, the electrons accumulate in the nanocrystal and the electron occupancy depends on the bias voltage between the tip and the substrate.[13, 14]

These limiting cases of tunnelling spectroscopy on nanocrystals allow us to see the link to electrochemical measurements on MPCs. In that case, the tunnelling rate out the MPCs is zero and by changing the voltage of the working

electrode, we can add or remove electrons to the MPCs one-by-one. This is true for both freely diffusing MPCs and those immobilized on substrate electrodes. The energy spacing between two electron additions is given by $\Delta E + E_c$. More specifically, the first electron addition occurs at electrochemical potential of[14-16]

$$\widetilde{\mu}_{0/-1} = E_{\mathrm{LUMO}} + \Sigma_e \quad (1)$$

where E_{LUMO} is the energy of the lowest unoccupied molecular orbital (LUMO) vs. the reference electrode. The added electron charge will polarize the dielectric medium of the nanocrystal (dielectric permittivity $\varepsilon_{\mathrm{in}}$) and the dielectric environment ($\varepsilon_{\mathrm{out}}$). Due to the fact that the dielectric screening length is larger than the radius of the nanocrystal, the charge of the incoming electron induces a negative charge density on the nanocrystal surface. The repulsion between the electron charge and induced surface charge is accounted for by the self-energy or polarization energy Σ_e.[14, 15] The second added electron will also occupy the LUMO orbital and energy required (neglecting spin interactions which are usually small compared to the level spacing and charging energy) is given by[14-16]

$$\widetilde{\mu}_{-1/-2} = E_{\mathrm{LUMO}} + \Sigma_e + E_c \quad (2)$$

where E_c is the electron-electron repulsion energy or the charging energy, i.e. the Coulomb repulsion between the added electrons. The third added electron will occupy the second unoccupied orbital (LUMO+1) with an energy of[14-16]

$$\widetilde{\mu}_{-2/-3} = E_{\mathrm{LUMO+1}} + \Sigma_e + 2E_c \quad (3)$$

Electron removal will occur from the highest occupied orbital (HOMO) at an energy of[14-16]

$$\widetilde{\mu}_{0/1} = E_{\mathrm{HOMO}} - \Sigma_h \quad (4)$$

where Σ_h is the polarization energy due to a hole. The energy difference between the first electron addition and removal (electrochemical gap) is different from the HOMO-LUMO gap due to the polarization energies and is given by

$$\Delta V_{ec} = \widetilde{\mu}_{0/-1} - \widetilde{\mu}_{0/1} = E_{LUMO} - E_{HOMO} + \Sigma_e + \Sigma_h \quad (5)$$

For nanocrystals with a high dielectric permittivity (such as metals), $\Sigma_e = \Sigma_h = E_c / 2$ to a good approximation.[14] If the level spacing is small (larger metallic particles), the electrochemical gap is simply given by E_c as expected. We will give details in the subsequent sections on how to estimate E_c for MPCs in an electrolyte solution.

Finally, the electrochemical gap can be compared to the optical gap which is given by (for an excitation of an electron from the HOMO to LUMO)[14]

$$\Delta V_{opt} = E_{LUMO} - E_{HOMO} + \Sigma_e + \Sigma_h - E_{e-h} = \Delta V_{ec} - E_{e-h} \quad (6)$$

where $E_{e\text{-}h}$ is the electron-hole attraction energy. To a good approximation, $E_{e\text{-}h} \approx E_c$.[14]

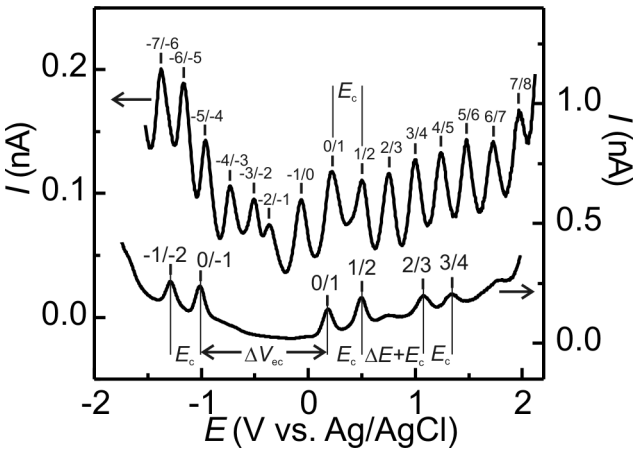

Fig. 3 DPV responses for MPC solutions measured at a Pt microelectrode; as-prepared 177 μM C6S-$Au_{\sim 140}$ (upper) showing 15 high-resolution QDL peaks and 170 μM C6S-Au_{38} (lower) showing an electrochemical HOMO-LUMO gap. The charging energy E_c is related to the voltage interval between current peaks ($E_c = e\Delta V$). For Au_{38}, the energy spacing between two electron additions is given by $\Delta E + E_c$. Reprinted from Ref. 17 with permission from the American Chemical Society.

Charging of freely diffusing MPCs

As discussed in the previous section, metal particles do not show quantum confinement effects comparable to semiconductor QDs unless the core diameter is in the sub-nanometre range. However, due to the sub-attofarad capacitance of monolayer-protected metal clusters (C_{MPC}), the electrostatic energy required to add an electron E_c can greatly exceed the thermal energy at room temperature even for clusters with a larger diameter. This means that the charge of the core can be controlled and discrete electron transfer can be observed. In a seminal contribution from Murray and co-workers, it was demonstrated that monodisperse thiol protected gold nanoparticles exhibit quantised charging in electrochemical experiments.[8] This study showed that solution dispersed particles can be treated as redox mediators in classical electrochemical experiments such as differential pulse voltammetry (DPV) and the current peaks observed in the current – voltage plots are due to single electron transfers between the metal electrode and the solution dispersed particles. As shown in Figure 3, up to 15 charging peaks can be readily resolved at room temperature for monodisperse hexanethiol (C6S) protected 1.7 nm diameter Au nanoparticles ($Au_{\sim 140}$) dispersed in 1,2-dichloroethane at a Pt microelectrode.[17] Each peak corresponds to single electron transfers between the diffusing MPCs and the metal electrode at the electrode/solution interface (Figure 2d). Even in the absence of quantum confinement effects, MPCs behave as multivalent redox species where the charge states z / $z \pm 1$ are separated by approximately regular voltage intervals $\Delta V = E_c/e$. It should be reiterated that monodispersity is critical to the interpretation of charging in terms of core size and indeed, to observation of quantized charging.[6] If the core size is reduced sufficiently, effects due to increased energy levels spacing become observable even for metallic clusters. Very small metallic clusters behave analogously to molecules with

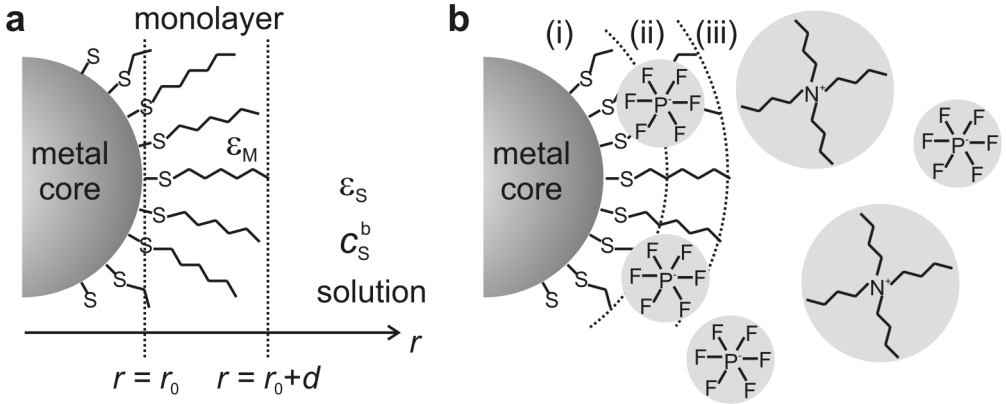

Fig. 4 (a) Schematic of the simple model showing a metal core coated by an impermeable monolayer immersed in a solvent containing base electrolyte. Reprinted from Ref. 17 with permission from the American Chemical Society. (b) Schematic illustration of the ion distribution around a positively charged MPC with counter-ion penetration to the monolayer. Area I denotes the extent of the ion-free monolayer, area II the extent of counter-ion penetration in the monolayer and area III the extent of the diffuse layer. Adapted from Ref. 18.

an energy gap opening between the occupied (HOMO) and unoccupied levels (LUMO).[8] This results in a large voltage gap (electrochemical HOMO-LUMO gap) between the first electron injection and removal in the electrochemical experiments as shown in Figure 3 (lower trace) for 1.1 nm core diameter MPCs (Au_{38}). The first and second added (removed) electrons occupy the same energy level and the voltage gap between them is due to capacitive charging of the core (i.e. the charging energy). In conclusion, for larger core diameters, electron addition / removal is purely a capacitive phenomenon while for sub-nm core diameters, the energetics are determined both by the spacing of the molecular energy levels and capacitive charging. C_{MPC} determines the charging energy and can be estimated from electrochemical measurements such as DPV from the voltage spacing between successive electron transfers $\Delta V = e/C_{MPC}$.[6, 8]

To be able to predict how C_{MPC} varies with core size, we need a model for the electrostatics of the charging of the core of the MPCs. The simplest model is a purely electrostatic one based on the concentric sphere capacitor proposed by Murray and co-workers.[6, 19] This approach was already used by Abeles et al. in 1973 to describe electron hopping in granular metal films.[20] Applying this to describe the MPC capacitance implicitly assumes that the effect of the electrochemical double layer set up by the electrolyte ions outside the protecting monolayer is negligible, and that the potential difference between the metal core and the surrounding medium is fully confined in the protecting monolayer.[19, 21]

The capacitance of the MPC according to this model can be determined using eq. (7).

$$C_{\mathrm{MPC}} = 4\pi\varepsilon_0\varepsilon_{\mathrm{m}}\frac{r_0}{d}(r_0 + d) \qquad (7)$$

where ε_m is the dielectric permittivity of the monolayer, r_0 the nanoparticle core radius, and d the length of the protecting ligands.[19] The three model parameters are core size, monolayer thickness and permittivity. Capacitance is assumed to be invariant with charge state z (i.e. the number of electrons added or removed from the core), and the monolayer is a simple dielectric barrier and medium effects are not included. r_0 and d are of the same order of magnitude and thus C_{MPC} increases with core radius and decreases with monolayer thickness.[19] The physical limits of C_{MPC} correspond to a naked nanoparticle in a bulk dielectric medium for $r_0 << d$ and to a thin monolayer on a flat surface for $r_0 >> d$.[21] A rule of thumb for the experimental observation of quantised charging is that ΔV should be greater than 6 k_BT/e (≈ 150 mV at room temperature) to be able to resolve individual peaks. For example, the experimental upper limit in terms of core radii for hexanethiolate and dodecanethiolate protected gold nanoparticles is ca. 1.2 and 1.4 nm, respectively. Eq. (7) predicts the charging behaviour remarkably well given the simplicity of the model.[21] The calculated capacitances are the correct order of magnitude and compare well with experimentally determined values. With the exception of the first oxidation and reduction, the agreement between theory and experiment is good for low charge states and predicts well the experimentally observed increase in capacitance with shorter ligand lengths and larger core radii.[6, 22] However, this model cannot account for all experimental observations, in particular the decrease in capacitance close to the potential of zero charge and variations seen at higher MPC charge states dependent on the solvent and base electrolyte used in the experiments.[21] The first effect is due to the electrical double layer surrounding the particle, and the second due to ion and solvent penetration into the ligand monolayer protecting the metal core.

The model has been extended to take medium effects into account.[17, 18, 21, 23-26] As charged particles always create an electric field around them, the solution phase cannot be considered a homogenous medium with a zero potential.[24] Girault and co-workers proposed that the solvent effect can be fully taken into account by a simple electrostatic model, where zero potential is not reached within the ligand monolayer, but at a distance far from the particle as it is done with a classical charged sphere.[23, 24] According to this model, the charged MPC is surrounded by the ligand monolayer and the solvent, which have different dielectric permittivity. This leads to an elegant equation, with a new parameter, the dielectric permittivity of the solvent, ε_s

$$\Delta V = \frac{e}{4\pi\varepsilon_0(r_0+d)}\left(\frac{l}{\varepsilon_m r_0}+\frac{1}{\varepsilon_s}\right) \quad (8)$$

This model is able to predict the experimentally reported dependence of ΔV on the solvent dielectric permittivity.[23, 24] However, like the simple model, eq. (7), it predicts an invariant ΔV with charge state and this is not in line with experimental data.[21]

To be able to predict the dependence of the MPC capacitance on the number of added electrons, it is essential to include the effect of the electrical double layer around the MPC.[17, 25, 26] The electrolyte ions feel the electric field created by the charged MPC, analogously to a macroscopic electrode where the electrolyte concentrations close to the surface change according to the well-known Gouy-Chapman theory.[17, 26] The capacitance of the Stern layer formed around the particle is of the same order of magnitude as that of the ligand monolayer. Thus, the monolayer capacitance, C_M, and electrical double layer capacitance, C_{dl} both contribute to C_{MPC} as given in eq. (9).

$$\frac{1}{C_{MPC}} = \frac{1}{C_M} + \frac{1}{C_{dl}} \quad (9)$$

This model requires the solution of the Poisson-Boltzmann equation, eq. (10), in radial coordinates.[17]

$$\begin{cases} \nabla^2\psi = -\dfrac{\rho}{\varepsilon} = \kappa^2 \sinh\left(\dfrac{F}{RT}\psi\right) \\ \dfrac{\partial}{\partial r}\psi\Big|_{r=a} = -\dfrac{ze}{4\pi\varepsilon_s\varepsilon_0 a^2} \end{cases} \quad (10)$$

where r is the radial coordinate, ψ is the potential, ρ is the charge density, σ is the surface charge density, z is the charge of the MPC, and a is the size of the particle i.e. $r_0 + d$. κ, the inverse of the Debye length, is defined as

$$\kappa = \sqrt{\frac{2F^2 c^b}{\varepsilon_s\varepsilon_0 RT}} \quad (11)$$

where c^b is the electrolyte bulk concentration. This involves solving the potential distribution around a charged sphere with an insulating shell. The equation must be solved for two areas simultaneously: the ligand monolayer and the solvent phase outside of the particles, with appropriate boundary conditions. It has been demonstrated that using planar coordinates will lead to significant errors, since the curvature at nanometre-sized particles is very high.[25] The linearised P-B equation has also been used though its use is questionable as typical nanoparticle surface potentials are at least an order of magnitude higher than the small perturbation potentials where the linear approximation is valid.[23]

The problem can be solved numerically to obtain the potential of the nanoparticle as a function of its charge. This model is an improvement on the previous models as it could also account for the influence of solvent permittivity and electrolyte concentration on the measured capacitance. The experimentally observed dip in C_{MPC} at the potential of zero charge as a function of electrolyte concentration could be successfully predicted using this model.[25] However, this model also assumes that the monolayer is an impermeable barrier to electrolyte ions and that the double layer is solely on the solution side of the MPC. Experimentally this is not the case as the charging of MPCs also depends on the nature (size) of the electrolyte ions.[18] The model can be refined by allowing the ions to penetrate the protecting monolayer. The electric field created by the charged MPC core can drag counter-ions from the solvent phase into the monolayer and this will affect C_{MPC} depending on ion size, hydrophobicity, monolayer thickness and permittivity and the solvent permittivity.

The ion permeability of the monolayer has been considered using two different approaches, one considering the depth to which the counter-ions penetrate the monolayer and the other considering the ion partition coefficient between the solution and monolayer phases.[18, 21] The former involves the solution of eq. (10) over three areas instead of two: the solvent phase and the electrolyte free and electrolyte penetrated monolayer phases as shown in the schematic in Figure 4b.[18] The ion penetration is characterized by the distance of closest approach of the ions to the core. The latter model can be solved numerically and the ion penetration is characterized by a partition coefficient K as given in eq. (12)[21]

$$\nabla^2\psi = -\frac{Fc^b}{\varepsilon_0\varepsilon_m}\left(K_+ e^{-F\psi/RT} - K_- e^{F\psi/RT}\right) \quad (12)$$

where K_i (i = +,-) is the ionic partition coefficient between the solution and the monolayer. Both approaches predict decreases in ΔV with increasing core charge when ions are present in the monolayer and can account for the experimental dependence of ΔV on the base electrolyte ions present in the dispersing solvent. The magnitude of the decrease depends on the extent to which the ions penetrate or partition into the monolayer. Experimentally, the monolayer permeability to a given ion is greatest in solvents with a low dielectric permittivity.[18] This can be rationalised by taking into account the energetics of ion solvation in the monolayer relative to the bulk solvent. The simple Born model can be used to give an estimate for the difference in the Gibbs energy of solvation ΔG for small ions in solvents of differing ε as follows[27]

$$\Delta_m^s G = -\frac{N_A z^2 e^2}{8\pi\varepsilon_0 r_{ion}}\left(\frac{1}{\varepsilon_s}-\frac{1}{\varepsilon_m}\right) \quad (13)$$

where subscripts m and s refer to the monolayer and solvent respectively and N_A is Avogadro's number.

According to eq. (13), a lower solvent dielectric permittivity would facilitate ion transfer from a solvent with ε comparable to that of the monolayer, which has been estimated to be <10. This prediction is in line with experimental data obtained where the solvent permittivity was varied. Eq. (13) is a very crude approximation as it does not include steric hindrance or the inhomogeneous nature of the ligand monolayer. However, the role of the solvation barrier

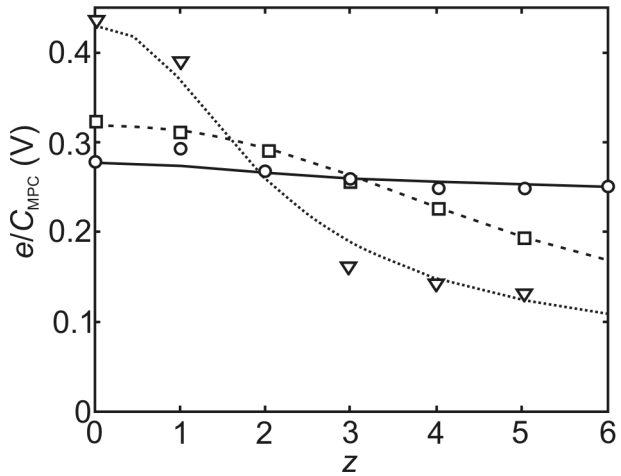

Fig. 5 Measured peak separation (symbols) values and the corresponding best fits obtained using the ion penetration model (lines) vs. particle charge state for identical MPCs dispersed in differing solvent/base electrolytes: tetraphenylarsonium tetrakis (pentafluorophenyl) borate ($TPAsTPBF_{20}$) in 1,2-dichloroethane (DCE) (circles and solid line), tetrabutylammonium hexafluorophosphate ($TBAPF_6$) in DCE (squares and dashed line), $TBAPF_6$ in chlorobenzene (triangles and dotted line). Reprinted from Ref. 21 with permission from the American Chemical Society.

for ion transfer across the solvent/monolayer interface can account for the influence of the dispersing solvent on the permeability of the monolayer to counter-ions. The lipophilicity and size of the counter-ions determine their ability to transfer across the solvation barrier.[27] The impact of ion lipophilicity depends on the relative solvation of the ion in the monolayer vs. the dispersing solvent. Given the thinness of the monolayer (0.77 nm for C6S), larger ions will have less influence as the charge centre is likely to be outside the monolayer and will not influence the monolayer permittivity as significantly as smaller ions

We summarize in the following how the various refinements to the simple concentric capacitor model compare with experimental data. The experimental variations in C_{MPC} that the model should be able to predict are summarised below:

1. The capacitance increases and thus ΔV decreases with increasing core size and decreasing monolayer thickness.[6, 19, 22, 28]
2. Increasing the dielectric permittivity of the solvent decreases ΔV.[18, 23-25]
3. There is a slight increase in ΔV around the zero charge state that is dependent on electrolyte concentration.[17, 18, 23-25]
4. ΔV is dependent on the nature of the base electrolyte ions at high charge states, $|z| > 4$.[18, 25, 29] Also, typically for the same particles, ΔV is dependent on the charge sign of the particles, i.e. whether the particles are undergoing oxidation or reduction.[17]

The simple model can only successfully predict (1) while the first refinement of the model which takes the solvent into account can also predict (2). (3) and (4) can only be reproduced by taking both the double layer and the ion permeability of the ligand monolayer into account. These observations are due to medium effects as explained above; the solvent and the base electrolyte used in the electrochemical measurements affect both the double layer and the barrier properties of the monolayer.

Effects (3) and (4) on MPC charging can be readily seen in Figure 5 where the same MPCs ($C6S\text{-}Au_{\sim 140}$) show markedly differing ΔV as a function of core charge simply by changing the solvent and base electrolyte ions.[18, 21] As base electrolyte is always added to solution in electrochemical experiments, the choice of electrolyte ions has a profound influence on the MPC charging response. It should be noted that ΔV is comparable for all base electrolytes in the same solvent for $z = 0$, i.e. ions do not enter the monolayer without an electrostatic driving force between the monolayer and bulk solution.[27] For the same particles dispersed in dichloroethane, ΔV differs by over 50 mV at $z = 5$ simply by changing the electrolyte anion from the large weakly coordinating tetrakis (pentafluorophenylborate) ($TPBF_{20}^-$) to the small hard hexafluophosphate (PF_6^-). The former case gives regularly spaced ΔV for $z > 0$ as the anion is too large to enter the monolayer while in the latter case, the ΔV decreases with each charge added due to PF_6^- entering the monolayer. In the latter case, simply changing the solvent from dichloroethane to the lower permittivity chlorobenzene also markedly affected ΔV both at $z = 0$ (double layer effects) and at higher charge numbers (ion penetration). For $z > 0$, anions will have a greater tendency to enter the monolayer and for $z < 0$, cations enter. Thus ΔV can be asymmetric around $z = 0$ if the cation and anion differ in terms of their ability to enter the monolayer. The extent of monolayer ion permeability is dependent on the core charge, the permittivities of the monolayer and the dispersing solvent and the base electrolyte ions in solution.[21] Irregularities in ΔV between the -1/-2 charge states have been ascribed to film formation where the MPCs precipitate onto the electrode surface due to solubility limitations in the solvent used.[17, 26]

Summarising, the energetics of MPC charging in solution are determined by the capacitance. It is primarily a function of the core size and the nature of the protecting monolayer. However, depending on the solvent and base electrolyte ions, the capacitance can be significantly altered by medium effects.

Films of immobilized MPCs on electrodes

In the previous section, we have discussed charging of freely diffusing MPCs. We next consider what factors influence charging when the MPCs are immobilised on the electrode surface.

There are several options for immobilizing MPCs on surfaces and here we briefly discuss the relative merits of the most widely used methods. The simplest method is drop-casting a film of particles from a concentrated solution onto the surface (Figure 6a). Advantages of this method are its simplicity and the possibility of generating thick films. The limitation is the absence of control of either film thickness or homogeneity. Also, the film can only be contacted with solvents into which the film does not dissolve. A more

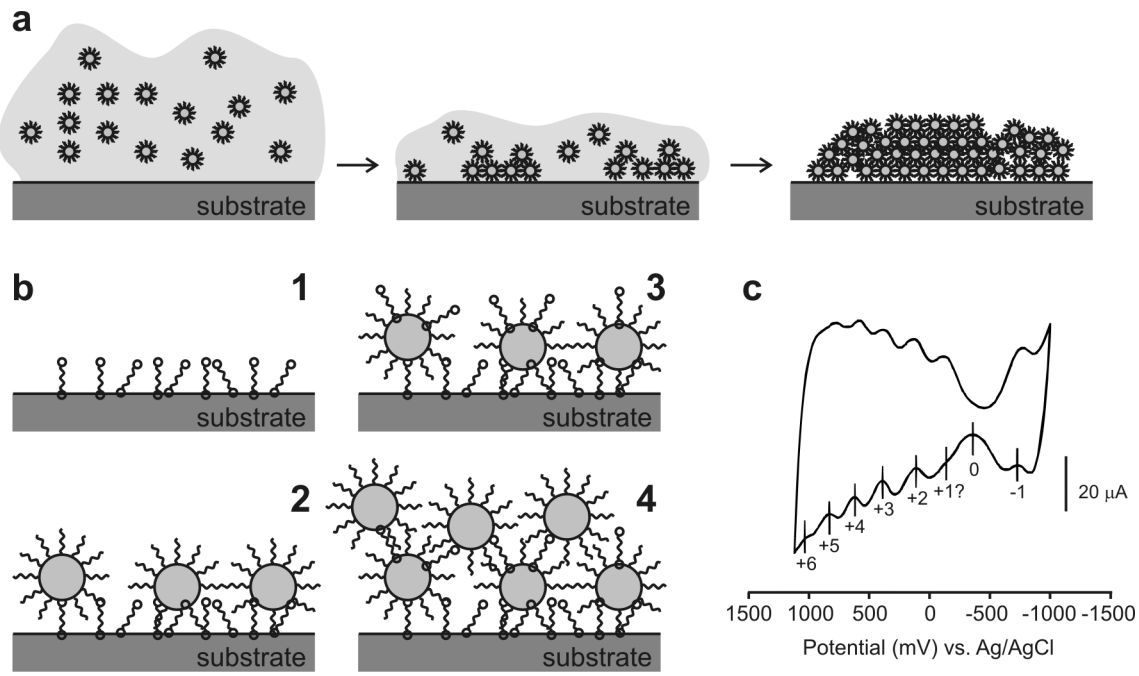

Fig. 6 (a) Cartoon showing creation of a multilayer MPC film by simple drop-casting: a droplet of MPCs dispersed in a solvent is deposited on the substrate. Evaporation of the solvent leads to the formation of a close-packed MPC assembly. (b) Schematic of a layer-by-layer assembly of MPCs using bifunctional linkers such as dithiols. The substrate is first functionalised by the bifunctional linkers (1), followed by alternating exposure to MPC dispersion (2, 4) and a solution of the linker molecules (3). (c) CV of a 300-nm-thick film of hexanethiolate-protected Au MPCs anchored by C10 dithiol linkers on a Au electrode in 0.1 M $TBAPF_6/CH_2Cl_2$ solution. Reprinted from Ref. 30 with permission from the American Chemical Society.

controlled method involves using dithiols as bifunctional linkers to chemically attach the MPC to a surface of usually an Au electrode (Figure 6b). The method works best when the aim is to generate low density mono- and bilayers on the electrode surface as the place-exchange of thiols on the surface of the MPCs is slow. The advantage of this method is that the particles are chemically linked to the surface and there are no restrictions on the solvents that can be contacted with the assembly. Other layer-by-layer approaches have also been used to obtain MPC assemblies utilizing the specific interactions between charged MPC peripheral groups and suitable linker molecules e.g. the chelating interactions between divalent metal cations and the carboxylic groups of MPCs and electrodes coated with carboxyalkanethiolates. In contrast to the dithiol linked MPC films, thick films can be readily achieved by these methods. As electrostatic interactions link the MPCs, the films are less stable than the chemically bonded dithiol linked films.

Typically when MPCs are immobilised on an electrode surface and immersed in low polarity electrolyte solutions, the MPC film voltammetry is analogous to that observed for the freely diffusing MPCs in the same solvent electrolyte system as shown in Figure 6c.[30] This is true for both monolayer and multilayer MPC assemblies.[30-32] MPC films can be considered as ideal electroactive thin films if the rate of electron transport in the film is not limiting.[33] However, for thicker films, the charging of the film is limited by the electron transport in the film and the observed response depends on the sweep rate. While the resolution of the charging peaks is dependent on the method used to immobilise the MPCs on the electrode surface, well-defined, roughly evenly spaced charging peaks are apparent throughout the potential window.[30-32] Irrespective of the linking chemistry, ΔV and thus C_{MPC}, is very similar to that observed for the solution phase MPCs.[30-32] The similarity to the solution phase voltammetry is such that a decrease in ΔV with increasingly positive MPC charge state is also apparent in the CV of a dithiolate-linked MPC film in $TBAPF_6/CH_2Cl_2$ solutions (Figure 6c).[30] This indicates that charge compensating counter-ions are readily available to maintain the electroneutrality of the film upon charging and that the film is solvated well by the low dielectric permittivity solvents used.

However, when MPC films are immersed in aqueous electrolyte solutions, the charging response is markedly different.[34, 35] As can be seen in Figure 7a (black solid lines), well-defined voltammetric peaks are apparent only at positive potentials in the presence of the relatively hydrophilic aqueous phase anions PF_6^-, ClO_4^-, BF_4^-, NO_3^-. The peaks have been ascribed to MPC oxidation and to date, reductive charging has not been reported for films immersed in aqueous electrolyte.[34-36] The onset potential where oxidation is initiated is strongly dependent on the nature and concentration of electrolyte anions added to solution.[35] This phenomenon is general and has been reported for various monolayer and multilayer MPC assemblies in a wide range of aqueous electrolyte media and has been termed "ion-induced rectification".[35]

Specifically, the onset potential for the first oxidation is dependent on the hydrophobicity of the anion and shifts to more negative potentials with increasing anion hydrophobicity in the following order $NO_3^- < BF_4^- < ClO_4^- < PF_6^-$ (Figure 7a). For a given anion, the peak potentials shift cathodically 59

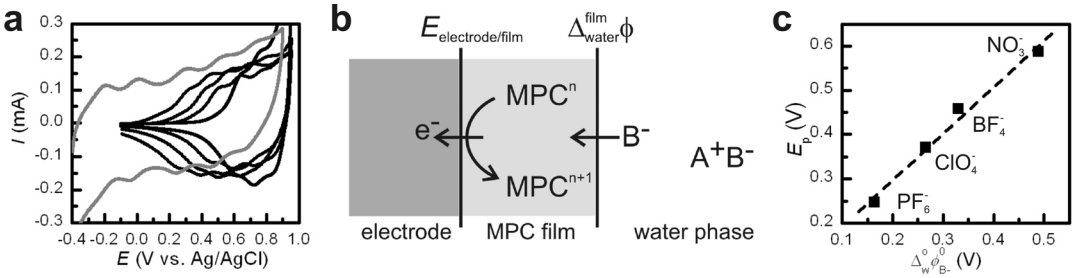

Fig. 7 (a) CVs of a drop cast film of hexanethiolate-protected Au MPCs on a gold electrode in aqueous solutions containing: from left to right: 20 mM $LiTPBF_{20}$ and 80 mM sodium acetate, 0.1 M NH_4PF_6, 0.1 M NH_4ClO_4, 0.1 M NH_4BF_4 and 0.1 M NH_4NO_3. Scan rate = 25 mV s^{-1}. (b) Schematic illustration of coupled electron and ion transfers for the oxidative charging of hydrophobic MPC films in aqueous solution (c) Dependence of MPC oxidation peak potential on the formal anion transfer potential across the water/dichlorobenzene interface of the aqueous anion used. Reprinted from Ref. 37 with permission from the American Chemical Society.

mV per decade increase in anion concentration. The peak spacing between successive electron transfers is also significantly decreased compared to the corresponding measurement performed in organic solvents.[35, 36] Generally, in low permittivity solvents, ΔV for MPC assemblies is comparable to that measured for freely diffusing particles, while in high permittivity solvents, it is considerably reduced.[30, 35, 36]

As the shifts in the onset potential with the nature and concentration of the anion are analogous to those seen in the voltammetry of conventional redox species when the base electrolyte ions ion-pair with the redox species,[33] it was initially explained within the framework of ion association. In this case, the ion-pair is the positively charged MPC – electrolyte anion (MPC^+-B^-) and the formation of the ion-pair was proposed to change the electrode interfacial double-layer capacitance.[34, 35] According to this model, the influence of the nature of the anion on the facilitation of MPC oxidative charging is due to the differing MPC^+-B^- association constants, with more hydrophobic ions binding more strongly thereby shifting the MPC potential of zero charge to lower values.[35] Experimentally, the electrolyte cation used also influences the onset potential for oxidative charging and the effect is dependent on the interplay between the relative lipophilicities of the anion and cation.[35] It is difficult to rationalise this effect within the framework of ion association as intuitively, cations regardless of lipophilicity or solvation structure are very unlikely to associate with positively charged species.

It should be reiterated that MPC are not conventional molecules and it is difficult to define a "distance of closest approach" for ion-pairing theories such as that of Bjerrum and Fuoss.[33] Conventional ion pairing giving an MPC^+B^- ion pair where the anion is located at the periphery of the monolayer protecting the metal core has no discernible effect on the MPC capacitance.[18, 21] As the redox properties of the MPC are determined by its capacitance, this type of ion pairing cannot explain the experimental data. Also the ion association model predicts that very hydrophobic anions should have highest association constant with MPC^+ and thus the most marked effect on MPC capacitance. However, it has been experimentally demonstrated that large hydrophobic ions do not influence the MPC capacitance as they do not penetrate the protecting monolayer and thus using the association model terminology, do not ion pair at all with MPCs.[18]

Thus, while the ion association model can qualitatively explain some of the observed phenomena, it suffers from some intrinsic limitations. For instance, ion-induced rectification implies that identical behaviour should be observed regardless of the solvent or the MPC monolayer hydrophobicity and this is not observed experimentally.[30, 38] Shifts in the position of the first oxidation peak have never been observed for MPCs in solution or comparable MPC films in organic solvents in the presence of the same electrolyte anions. Finally, the concept of "electrochemically active layers" was introduced to explain the large discrepancies between the MPC surface coverage determined from voltammetric or quartz crystal microbalance (QCM) measurements implying that anion association and hence MPC charging occurs only at the top few layers of multilayer films and the bottom layers simply transfer the charge to the electrode.[36]

This ion-pairing based interpretation does not take into account the solvation barrier for the transfer of charge compensating counter-ions into the film when the particles are oxidized.[39] The MPC film is essentially a thin organic phase as illustrated schematically in Figure 7b and the immiscible interface formed upon contacting it with the aqueous phase has to be taken into account as current has to be carried across this interface.[37, 39] The energy required to transfer an ion across this boundary is related to the differences in ion solvation in the respective media.[27] These differences are significant and can control the apparent redox properties of MPC thin films.[39] The particles are multivalent redox centres that undergo electron transfer at the metal electrode surface while the film/solution interface is a solvation barrier to the transfer of charge compensating ions into the film.[37]

We will briefly outline the concept of coupled ion transfer (IT) and electron transfer (ET) to illustrate how the MPC charging at the electrode surface is not possible without the transfer of counter-ions across the film/solution interface to preserve the electroneutrality of the film. The experimental peak potential is thus determined by both the redox reaction and the ion transfer reaction.[39] The overall electrode reaction for the oxidation of film MPCs in an aqueous electrolyte A^+B^- is as follows:

$$\mathrm{MPC}^{\,n}_{\,film} + \mathrm{B}^-_w \Leftrightarrow \mathrm{MPC}^{\,n+1}_{\,film} + \mathrm{B}^-_{film} + e^-_M \qquad (14)$$

where the transfer of the anion B^- from the aqueous phase to the film phase is the coupled IT reaction.[37] The charging of the MPCs at the film/electrode interface serves as the driving force for ion transfer across the film/solution interface. The overall reaction couples these processes, which occur simultaneously and cannot be separated. As the film is conductive, ohmic loss in the film is not limiting.

The potential difference established across the film/solution interface $\Delta^{film}_{w}\phi$ is dependent on the relative hydrophobicity of the constituent anions and cations.[27] Charge transfer across this interface is not a redox process and is simply a measure of the relative solvation properties of the transferring ionic species in each phase.[27] $\Delta^{film}_{w}\phi$ can be written as follows:

$$\Delta^{film}_{w}\varphi = \phi^{film} - \phi^{w} = \Delta^{film}_{w}\phi^{0'}_{B^-} + \frac{RT}{F}\ln\frac{[B^-_{film}]}{[B^-_w]} \qquad (15)$$

where $\Delta^{film}_{w}\phi^{0'}_{B}$ is the formal transfer potential for the anion, and $[B^-_{film}]$ and $[B^-_w]$ are the film and solutions concentrations respectively.[27] It is assumed that the film is homogeneous. The applied potential E is the sum of the potential drop across the electrode/film and film/solution interfaces[39]

$$E = E_{electrode\ /\ water} = E_{electrode\ /\ film} + \Delta^{film}_{w}\phi \qquad (16)$$

At equilibrium, overall reaction (14) can be described by the Nernst equation:

$$E = E^{0'} + \Delta^{film}_{w}\phi^{0'}_{B^-} + \frac{RT}{F}\ln\frac{[\mathrm{MPC}^{n+1}][B^-_{film}]}{[\mathrm{MPC}^{n}][B^-_w]} \qquad (17)$$

where $E^{0'}$ is the formal potential for MPC charging and $[MPC^n]$ and $[MPC^{n+1}]$ are the concentrations of the charged MPC species inside the film.[37] We can rewrite eq. (17) in terms of the half-wave potential

$$E_{1/2} = E^{0'} + \Delta^{film}_{w}\phi^{0'}_{B^-} + \frac{RT}{F}\ln\left(\frac{2n+1}{2}[\mathrm{MPC}_{tot}]\right) - \frac{RT}{F}\ln[B^-_w] \qquad (18)$$

where $[MPC_{tot}]$ is the total nanoparticle concentration in the film.[37] Thus, a 10 fold increase in the anion concentration should shift the measured $E_{1/2}$ by 59 mV in a negative direction, identical to that predicted using the ion pairing model for 1:1 binding between the oxidized MPC and the aqueous anion.[35] Eq. (18) also shows how the measured $E_{1/2}$ depends on the nature of the aqueous anion via the transfer potential term. Generally, the formal transfer potential values decrease as anion hydrophobicity increases and vice versa for hydrophilic ions.[27] Consequently the oxidation of the MPC in the film will be shifted to more negative potentials when the lipophilicity of the anion increases.[37] The charging onset potentials can be compared to calculated $\Delta^{film}_{w}\phi^{0'}_{B^-}$ values using Gibbs energies of transfer between water and dichlorobenzene (DCB) ($\Delta^{o}_{w}\phi^{0}_{i} = \Delta G^{0,w\rightarrow o}_{tr,i} / z_i F$).[27, 37] While an MPC film is not strictly comparable to a simple solvent such as DCB, differences in Gibbs energies will be of the right magnitude and we should be the same order in the position of the onset potentials. Calculated standard transfer potentials for the four most commonly used anions were 165 mV (PF_6^-), 266 mV (ClO_4^-), 331 mV (BF_4^-) and 489 mV (NO_3^-).[37] This is the same order that is seen experimentally. The plot of peak potentials obtained in the presence of each ion (extrapolated to $\ln[B_w^-] = 0$) vs. their respective standard ion transfer potentials given in Figure 7c is linear with a slope of 1 as predicted by eq. (18).

Thus, the onset potential of the film charging is controlled by the solvation barrier to ion transfer at the film/water interface. The observed response should be highly dependent on both the solvent and the hydrophobicity of the aqueous phase anion. Both effects have been reported in the literature.[35,37] Rectification is not observed for films immersed in low dielectric permittivity solvents like dichloroethane as there is no solvation barrier between the film and solution phases.[30, 35] The influence of anion hydrophobicity can be directly seen when the CV responses obtained for identical films immersed in aqueous solution containing either a moderately hydrophilic anion PF_6^- or a very hydrophobic anion, pentafluorotetraphenylborate ($TPBF_{20}^-$, grey line) are compared as in Figure 7a.[37] The PF_6^- case shows a clear onset for charging as it does not transfer until $\Delta^{film}_{w}\phi > \Delta^{film}_{w}\phi^{0'}_{PF_6^-}$. Until this criterion is fulfilled, electron transfer is also shut off and the measured current is zero. In contrast, for the $TPBF_{20}^-$ case, there is no onset potential for MPC charging and peaks are apparent throughout the available potential window. The response is comparable to that obtained for dispersed particles in dichloroethane. $\Delta^{film}_{w}\phi^{0'}_{TPBF_{20}^-} << 0$ and $\Delta^{film}_{w}\phi > \Delta^{film}_{w}\phi^{0'}_{TPBF_{20}^-}$ for all applied potentials within the available potential window. Thus, hydrophobic $TPBF_{20}^-$ transfers into the film at all interfacial potentials as was confirmed by the mass changes observed in the *in situ* quartz crystal microbalance measurements recorded simultaneously. Mass changes are seen throughout the window for $TPBF_{20}^-$ and only after the onset potential has been reached for PF_6^-.[37]

The ion transfer limited model can account for the dependence of MPC oxidative charging on the nature and concentration of the aqueous anion without invoking any a priori interaction between the MPC and the counter-ion. It can quantitatively explain shifts in apparent film redox potentials with differing anions. Coupled ion and electron transfer should also be equally applicable for reductive MPC charging. However, reduction peaks are absent even when suitably lipophilic cations like tetraethylammonium are added to the aqueous solution[35]. The absence of reduction charging peaks for MPC films immersed in aqueous solutions is intriguing and currently there is no explanation for this.

Conclusions

Quantised charging is a general feature of electron injection/removal to/from nanometre-sized particles. Depending on the core material and size, the energetics of electron transfer are determined either by pure electrostatics or by both electrostatics and quantum confinement effects. The charging energy is controlled by the nanoparticle capacitance; MPCs with radii of < 1 nm have capacitance below 1 aF and exhibit resolvable charging peaks in current-voltage plots at room temperature. The value of the

capacitance is determined primarily by the core size and the dielectric permittivity of the protecting monolayer. Quantised charging of MPCs can be experimentally realised in conventional electrochemical experiments simply by using the particles as redox mediators in solution or as redox active films immobilized onto an electrode surface. The simple concentric capacitor model predicts the correct order of magnitude for the MPC capacitance and the variation in C_{MPC} with core diameter and monolayer thickness. However, it has been experimentally shown that the MPC capacitance is also dependent on the solvent and the base electrolyte, in contradiction with the concentric capacitor picture. The base electrolyte ions can penetrate into the protecting monolayer around the MPCs and the magnitude of this effect is governed both by ion size and hydrophobicity. For MPC films, the transfer of charge compensating counter-ions across the phase boundary between the film and the electrolyte solution can control MPC charging.

Acknowledgements

We acknowledge financial support from the University of Helsinki (Development of Nano Sciences/HENAKOTO, 700036, T.L.), Academy of Finland (Academy Research Fellow, B.M.Q.), Nederlandse Organisatie voor Wetenschappelijk Onderzoek (NWO/Chemical Sciences, Vidi-grant 700.56.423, P.L.), and the Ministerio de Educacio´n y Ciencia (Juan de la Cierva contract, V.R.)

Notes and references

[a] *Division of Pharmaceutical Technology, Faculty of Pharmacy, University of Helsinki, PO Box 56, FIN-00014 University of Helsinki, Finland..*
[b] *Department of Chemistry, University of Burgos, Pza. Misael Banuelos, s/n, Burgos 09001 Spain.*
[c] *Condensed Matter and Interfaces, Debye Institute, University of Utrecht, PO Box 80000, 3508 TA Utrecht, the Netherlands.*
[d] *Department of Chemistry, Helsinki University of Technology, PO Box 6100, FIN-02015 HUT, Finland.*

1. A. P. Alivisatos, *J. Phys. Chem.*, 1996, **100**, 13226-13239.
2. L. P. Kouwenhoven, D. G. Austing and S. Tarucha, *Rep. Prog. Phys.*, 2001, **64**, 701-736.
3. C. B. Murray, C. R. Kagan and M. G. Bawendi, *Ann. Rev. Mat. Sci.*, 2000, **30**, 545.
4. A. Henglein, *Chem. Rev.*, 1989, **89**, 1861-1873.
5. M. Brust, M. Walker, D. Bethell, D. J. Schiffrin and R. Whyman, *J. Chem. Soc. Chem. Commun.*, 1994, 801-802.
6. A. C. Templeton, W. P. Wuelfing and R. W. Murray, *Acc. Chem. Res.*, 2000, **33**, 27-36.
7. M.-C. Daniel and D. Astruc, *Chem. Rev.*, 2004, **104**, 293-346.
8. S. W. Chen, R. S. Ingram, M. J. Hostetler, J. J. Pietron, R. W. Murray, T. G. Schaaff, J. T. Khoury, M. M. Alvarez and R. L. Whetten, *Science*, 1998, **280**, 2098-2101.
9. *Single Charge Tunneling*, eds. H. Grabert and M. H. Devoret, Plenum, New York, 1992.
10. D. L. Klein, R. Roth, A. K. L. Lim, A. P. Alivisatos and P. L. McEuen, *Nature*, 1997, **389**, 699-701.
11. R. P. Andres, T. Bein, M. Dorogi, S. Feng, J. I. Henderson, C. P. Kubiak, W. Mahoney, R. G. Osifchin and R. Reifenberger, *Science*, 1996, **272**, 1323-1325.
12. U. Banin and O. Millo, *Ann. Rev. Phys. Chem.*, 2003, **54**, 465-492.
13. P. Liljeroth, L. Jdira, K. Overgaag, B. Grandidier, S. Speller and D. Vanmaekelbergh, *Phys. Chem. Chem. Phys.*, 2006, **8**, 3845 - 3850.
14. C. Delerue and M. Lannoo, *Nanostructures-Theory and Modelling*, Springer-Verlag, Berlin, 2004.
15. A. Franceschetti, A. Williamson and A. Zunger, *J. Phys. Chem. B*, 2000, **104**, 3398-3401.
16. D. Vanmaekelbergh and P. Liljeroth, *Chem. Soc. Rev.*, 2005, **34** 299-312.
17. B. M. Quinn, P. Liljeroth, V. Ruiz, T. Laaksonen and K. Kontturi, *J. Am. Chem. Soc.*, 2003, **125**, 6644-6645.
18. T. Laaksonen, O. Pelliniemi and B. M. Quinn, *J. Am. Chem. Soc.*, 2006, **128**, 14341-14346.
19. S. Chen, R. W. Murray and S. W. Feldberg, *J. Phys. Chem. B*, 1998, **102**, 9898-9907.
20. P. Sheng, B. Abeles and Y. Arie, *Phys. Rev. Lett.*, 1973, **31**, 44-47.
21. V. Garcia-Morales and S. Mafe, *J. Phys. Chem. C*, 2007, **111**, 7242-7250.
22. J. F. Hicks, A. C. Templeton, S. Chen, K. M. Sheran, R. Jasti, R. W. Murray, J. Debord, T. G. Schaaff and R. L. Whetten, *Anal. Chem.*, 1999, **71**, 3703-3711.
23. B. Su, M. Zhang, Y. Shao and H. H. Girault, *J. Phys. Chem. B*, 2006, **110**, 21460-21466.
24. B. Su and H. H. Girault, *J. Phys. Chem. B*, 2005, **109**, 23925-23929.
25. R. Guo, D. Georganopoulou, S. W. Feldberg, R. Donkers and R. W. Murray, *Anal. Chem.*, 2005, **77**, 2662-2669.
26. D. T. Miles and R. W. Murray, *Anal. Chem.*, 2003, **75**, 1251-1257.
27. *Liquid-liquid interfaces, Theory & Methods*, eds. A. G. Volkov and D. W. Deamer, CRC Press, Boca Raton, 1996.
28. M. J. Hostetler, J. E. Wingate, C.-J. Zhong, J. E. Harris, R. W. Vachet, M. R. Clark, J. D. Londono, S. J. Green, J. J. Stokes, G. D. Wignall, G. L. Glish, M. D. Porter, N. D. Evans and R. W. Murray, *Langmuir*, 1998, **14**, 17-30.
29. J. F. Hicks, D. T. Miles and R. W. Murray, *J. Am. Chem. Soc.*, 2002, **124**, 13322-13328.
30. J. L. Brennan, M. R. Branham, J. F. Hicks, A. J. Osisek, R. L. Donkers, D. M. Georganopoulou and R. W. Murray, *Anal. Chem.*, 2004, **76**, 5611-5619.
31. F. P. Zamborini, J. F. Hicks and R. W. Murray, *J. Am. Chem. Soc.*, 2000, **122**, 4514.
32. S. Chen and R. W. Murray, *J. Phys. Chem. B*, 1999, **103**, 9996.
33. A. J. Bard and L. R. Faulkner, *Electrochemical methods, Fundamentals and applications*, 2nd edn., John Wiley & Sons Inc., New York, 2001.
34. S. Chen, *J. Am. Chem. Soc.*, 2000, **122**, 7420-7421.
35. S. Chen and R. Pei, *J. Am. Chem. Soc.*, 2001, **123**, 10607-10615.
36. F. Deng and S. Chen, *Langmuir*, 2007, **23**, 936-941.
37. T. Laaksonen, V. Ruiz, L. Murtomaki and B. M. Quinn, *J. Am. Chem. Soc.*, 2007, **129**, 7732-7733.
38. S. D. Jhaveri, D. A. Lowy, E. E. Foos, A. W. Snow, M. G. Ancona and L. M. Tender, *Chem. Commun.*, 2002, 1544.
39. F. Scholz and R. Gulaboski, *Chem. Phys. Chem.*, 2005, **6**, 16-28.